

# Geophysical Research Letters<sup>®</sup>

## RESEARCH LETTER

10.1029/2022GL100742

### Key Points:

- Tree rings better represent baseflow compared to stormflow and total streamflow
- Rapid 20th–21st century increases in baseflow escalate flooding susceptibility and are exceptional over the last 1,118 years
- Recent increases in baseflow are related to the position of the western flank of the North Atlantic subtropical high

### Supporting Information:

Supporting Information may be found in the online version of this article.

### Correspondence to:

J. T. Maxwell,  
maxweljt@indiana.edu

### Citation:

Maxwell, J. T., Harley, G. L., Tucker, C. S., Galuska, T., Ficklin, D. L., Bregy, J. C., et al. (2022). 1,100-year reconstruction of baseflow for the Santee River, South Carolina, USA reveals connection to the North Atlantic subtropical high. *Geophysical Research Letters*, 49, e2022GL100742. <https://doi.org/10.1029/2022GL100742>

Received 9 AUG 2022

Accepted 9 NOV 2022

### Author Contributions:

**Conceptualization:** Justin T. Maxwell, Grant L. Harley

**Formal analysis:** Justin T. Maxwell, Toudora Galuska, Darren L. Ficklin

**Funding acquisition:** Justin T. Maxwell, Grant L. Harley, Emily A. Elliott, Matthew D. Therrell

**Investigation:** Joshua C. Bregy, Karen J. Heeter, Tsun Fung Au, Benjamin R. Lockwood, Daniel J. King, R. Stockton Maxwell, Laura G. Smith

**Methodology:** Justin T. Maxwell, Darren L. Ficklin











**Supervision:** Justin T. Maxwell, Grant L. Harley

**Visualization:** Grant L. Harley

**Writing – original draft:** Justin T. Maxwell, Clay S. Tucker

**Writing – review & editing:** Justin T. Maxwell, Grant L. Harley, Clay S. Tucker,

## 1,100-Year Reconstruction of Baseflow for the Santee River, South Carolina, USA Reveals Connection to the North Atlantic Subtropical High

Justin T. Maxwell<sup>1</sup> , Grant L. Harley<sup>2</sup> , Clay S. Tucker<sup>3,4</sup>, Toudora Galuska<sup>1</sup>, Darren L. Ficklin<sup>1</sup> , Joshua C. Bregy<sup>5,6</sup> , Karen J. Heeter<sup>2</sup> , Tsun Fung Au<sup>1,7,8</sup> , Benjamin R. Lockwood<sup>1</sup>, Daniel J. King<sup>2</sup> , R. Stockton Maxwell<sup>9</sup> , Laura G. Smith<sup>10</sup>, Emily A. Elliott<sup>3</sup> , and Matthew D. Therrell<sup>3</sup> 

<sup>1</sup>Department of Geography, Indiana University, Bloomington, IN, USA, <sup>2</sup>Department of Earth and Spatial Sciences, University of Idaho, Moscow, ID, USA, <sup>3</sup>Department of Geography, University of Alabama, Tuscaloosa, AL, USA, <sup>4</sup>School of Biological, Environmental, and Earth Sciences, University of Southern Mississippi, Hattiesburg, MS, USA, <sup>5</sup>Department of Environmental Engineering and Earth Science, Clemson University, Clemson, SC, USA, <sup>6</sup>Glenn Department of Civil Engineering, Clemson University, Clemson, SC, USA, <sup>7</sup>School for Environment and Sustainability, Institute for Global Change Biology, University of Michigan, Ann Arbor, MI, USA, <sup>8</sup>Department of Ecology and Evolutionary Biology, University of Michigan, Ann Arbor, MI, USA, <sup>9</sup>Department of Geospatial Science, Radford University, Radford, VA, USA, <sup>10</sup>Harvard Forest, Harvard University, Petersham, MA, USA

**Abstract** Since 2013, extreme floods within the Santee River basin (North/South Carolina, USA) caused \$1.5B in damage. The instrumental period, however, is too short to determine if recent extreme events are anomalous within a long-term context. Here, we present reconstructions of storm-, base-, and total streamflow for the Santee River using a multi-species tree-ring network calibrated to flow data during the period 1923–2018. Tree-ring data explained higher variance ( $r = 0.59$ ;  $p < 0.01$ ; 900–2018) of instrumental baseflow than total streamflow ( $r = 0.41$ ;  $p < 0.01$ ; 1500–2018) or stormflow ( $r = 0.26$ ;  $p < 0.05$ ; 1690–2018). Our reconstruction reveals a long-term increase in baseflow over the past millennium. The North Atlantic subtropical high regulates baseflow in the Santee River ( $r = 0.45$ ;  $p < 0.01$ ). Recent high levels of baseflow may be connected to the position of the subtropical high, increasing the likelihood of flooding.

**Plain Language Summary** Tree rings are often used to estimate past levels of streamflow to better place modern extremes into a historical context. Streamflow has two components, baseflow (flow from groundwater) and stormflow (flow contributed from storms). Here, we use tree rings to estimate past streamflow of the Santee River, South Carolina, USA. We find that tree rings are better at representing variations in baseflow rather than stormflow. This connection to baseflow is likely because tree growth is related to long-term changes in water supply throughout the growing season, and changes in baseflow are more likely to result in changes in annual growth. Additionally, we find that certain species are more sensitive to baseflow than others, with *Taxodium distichum* (bald cypress) being the most sensitive. We were able to reconstruct baseflow back 1,100 years and found that baseflows increased over this time. Higher levels of baseflow will result in larger flooding events, like the 2013 and 2019 events. The location of the western edge of a large atmospheric high pressure centered off the Atlantic Coast, the North Atlantic subtropical high, has a strong influence on baseflow levels and could explain the increasing trend in reconstructed baseflows.

## 1. Introduction

The southeastern United States (US) is dominated by moist, maritime air masses, and thus generally has large amounts of rainfall and plentiful water resources. However, increasing population and infrastructure in this region can lead to increases in flooding potential due to more impervious surfaces and at the same time, increases water demand (Gangrade et al., 2020; Nagy et al., 2011; Seager et al., 2009). Further, climate in this region also can lead to flooding and drought conditions. Rainfall rates in the southeastern US have been increasing (Ban et al., 2015; Trenberth et al., 2003), compounding issues of flash flooding due to increases in impervious surfaces in cities. Concurrently, temperatures in this region have increased, particularly nighttime temperatures, since the 1980s (Meehl et al., 2015; USGCRP, 2018), increasing water demand, which add to the strain on water resources from increasing population. However, high and low extremes in streamflow are infrequent, making it difficult to

Toudora Galuska, Darren L. Ficklin, Joshua C. Bregy, Karen J. Heeter, Tsun Fung Au, Benjamin R. Lockwood, Daniel J. King, R. Stockton Maxwell, Laura G. Smith, Emily A. Elliott, Matthew D. Therrell

determine how unusual observed extremes may be and how increases in population and infrastructure along with changes in the climate system influence those extremes.

Streamflow represents a combination of both baseflow and stormflow, and most often just baseflow for a large portion of the year. Baseflow originates from saturated soil and/or groundwater flow and slowly varies over time. Stormflow, on other hand, is of shorter duration and follows major precipitation events and often a larger volume than baseflow. Both components are a function of climate and basin characteristics. While flash flood events are best captured by stormflow, higher-than-usual baseflow can increase the susceptibility of flooding from relatively small rainfall events. The combination of increased rainfall rates (Ban et al., 2015; Trenberth et al., 2003) and slower, wetter tropical cyclones (Hall & Kossin, 2019; Maxwell et al., 2021; Trepanier & Tucker, 2018) is leading to increases in both stormflow and baseflow due the large amounts of rainfall and has resulted in more frequent flooding in coastal cities (Hall & Kossin, 2019; Maxwell et al., 2021). Thus, longer records of stormflow and baseflow are needed to better understand the extent and variability of both high and low extremes in streamflow. A better understanding of extremes and shifts in these streamflow metrics will allow for more accurate water management strategies and more resilient urban areas to current and impending anthropogenic climate change.

Tree rings can provide the needed longer-term perspective in streamflow variability and extremes, extending streamflow records by centuries to millennia (Harley & Maxwell, 2018; Wise, 2010; Woodhouse et al., 2006). While streamflow reconstructions were historically more prevalent in the arid western US, radial growth from trees has proven to be representative of streamflow in the wetter eastern US where summer streamflow is linked to large-scale climate patterns (Cook and Jacoby, 1977, 1983; Maxwell et al., 2011; Strange et al., 2019). While tree rings have been used to reconstruct total streamflow in parts of the southeastern US (Harley et al., 2017; Maxwell et al., 2017; Vines et al., 2021), only one study—of the Potomac River in the Mid-Atlantic US—has included separate records of stormflow and baseflow (Torbenson & Stagge, 2021).

Here, we used tree rings to reconstruct baseflow, stormflow, and total streamflow variability for the Santee River, South Carolina, US. The Santee River Basin encompasses 64,408 km<sup>2</sup> across North Carolina (NC) and South Carolina (SC) and includes the Broad, Catawba, Congaree, Saluda, and Wateree Rivers as tributaries, flowing over 700 km from headwaters to mouth. The Santee River travels through three physiographic provinces, starting in the Blue Ridge Mountains in NC and flowing through the Piedmont and Coastal Plains of the Carolinas before draining into the Atlantic Ocean (Figure 1). The stream has several dams throughout the middle and lower reaches that supply millions of people with municipal and drinking water. Three cities with populations greater than 50,000 are within this drainage basin, and the city of Columbia, SC falls within its floodplain. Understanding long term patterns of the Santee River is paramount for understanding risk from flooding and drought in the future. We examined whether tree-ring widths were more representative of baseflow, stormflow, or streamflow. We then explored long-term variability and large-scale climate controls on the most robust streamflow model.

## 2. Materials and Methods

### 2.1. Streamflow Data

Due to multiple anthropogenic alterations of the Santee River in the middle and lower reaches of the stream, we gathered mean monthly flow data from United States Geological Survey (USGS) gauge 02138500 near Nebo, NC on the Linville River—a stream gauge with relatively minimal influence related to human alterations (Figure 1). The gauge 02138500 is included in the USGS HydroClimatic Data Network (HCDN), a subset of minimally altered streams (Slack & Landwehr, 1992). Further, this stream gauge has one of the longest and most continuous records (1923–2018 CE), allowing for 96 years of data on which to calibrate our reconstruction model. The need to ensure that streamflow variability is predominantly related to natural climatic controls limited the target stream gauges to headwaters. Although in the headwaters, the interannual variability in streamflow at this gauge matched the downstream gauges. For example, the Linville River gauge has a significant correlation ( $r = 0.60$ ,  $p < 0.01$ ; 1930–2018 CE) with the USGS gauge 02148000 near Camden, SC on the Wateree River (Figure S1 in Supporting Information S1). The Wateree River stream gauge has the longest record among the gauges in the lower to middle reaches, but far enough upstream to not have a tidal signal. Thus, the use of the Linville River HCDN, which is the gauge with the longest record of all gauges and ensures that streamflow is responding to natural controls such as climatic variation but still represents the total streamflow of the basin well. We further examined seasonal averages of streamflow to match the growing season and determined it matched annual flow well

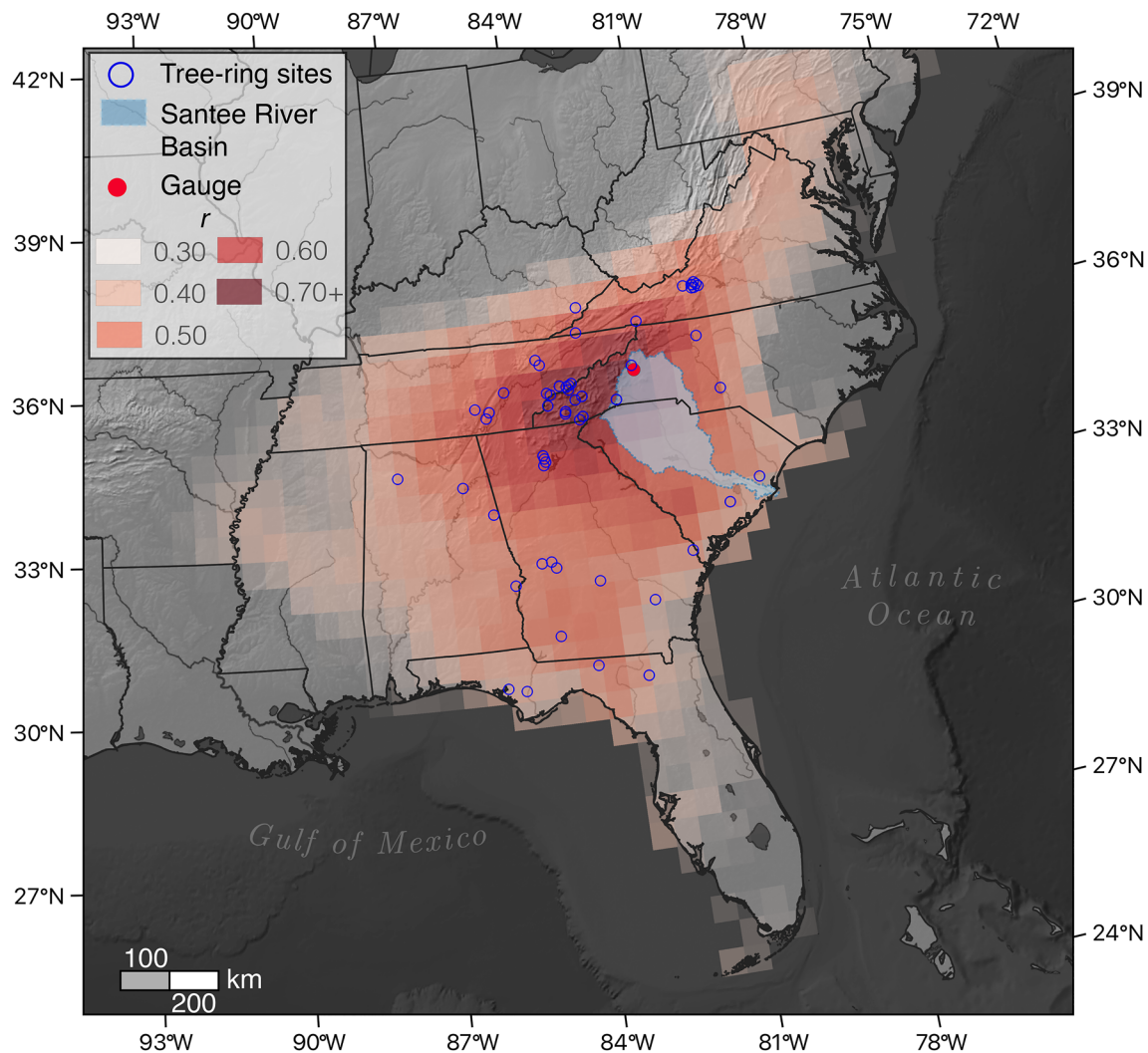


**Figure 1.** Geography of the Santee River basin and predictor chronologies across the southeast US. Map of Santee watershed (blue) and all tree-ring chronologies that are tested to be predictors of the streamflow metric reconstructions against the backdrop of the Linville River gauge “climate footprint”, viewed as the spatial correlation between average May–August gridded precipitation data from CRU TS4.04 (Harris et al., 2020) and average May–August streamflow from the Linville River gauge (red).

(Figures S2 and S3 in Supporting Information S1). Lastly, because trees can respond to current year ( $t$ ) and previous year ( $t-1$ ) climate in the eastern US (Kannenberg et al., 2019), we tested the autocorrelation function values for the instrumental and reconstructed streamflow for each metric (Figure S4 in Supporting Information S1).

To better examine the various components of streamflow and to determine the logistics of reconstructing each variable, we separated streamflow into stormflow and baseflow. We use the USGS automated baseflow-separation method HYSEP (hydrograph-separation; Sloto & Crouse, 1996) to extract baseflow from total streamflow. Specifically, we employed the local minimum HYSEP method, whereby each daily streamflow value was compared to the streamflow value on the previous and subsequent day (Sloto & Crouse, 1996). If the streamflow value was lower than the previous and subsequent day, the local streamflow minimum was connected by a straight line to other local streamflow minima in the time series, which was used to estimate the baseflow time series. From this time series, stormflow was estimated by subtracting baseflow from the total streamflow. Additional information can be found in Supporting Information S1.

## 2.2. Tree-Ring Data

We used a combination of new site collections and existing chronologies from the International Tree-Ring Data-bank (ITRDB; <https://www.ncdc.noaa.gov/data-access/paleoclimatology-data/datasets/tree-ring>) that are within and surrounding the Santee River Basin as possible predictors. One way tree-ring chronologies are used to reconstruct streamflow is by sampling from forest stands that are within the target drainage basin. In this case, there were few chronologies located within the basin, but there was positive spatial autocorrelation between climate inside and outside the delineated basin. Thus, we used the *climate footprint* (Harley et al., 2017; Maxwell et al., 2017) approach to select chronologies that experienced similar hydroclimatic conditions as the Santee River Basin. This approach was shown to provide a more robust representation of streamflow from tree rings rather than only selecting sites within the basin or applying an arbitrary buffer region from which to select predictors (Strange et al., 2019). The climate footprint entails conducting a spatial correlation analysis between the Linville River streamflow from the USGS gauge and gridded precipitation data from Climatic Research Unit (CRU) TS4.04 (Harris et al., 2020). We screened the number of possible chronologies to include in the reconstruction model by only selecting those chronologies that are in locations with a correlation coefficient  $\geq 0.5$  between averaged May–August precipitation and streamflow (Figure 1). In doing this, we increased the chance that the radial growth from these chronologies would be sensitive to precipitation in the same way that streamflow responds to changes in precipitation.

Many of the chronologies on the ITRDB were sampled in the 1980s, and therefore, limit the calibration length of reconstruction models, while also making it difficult to put recent variability into historical context. To account for this, we updated 11 ITRDB sites and sampled at three new sites so that we had tree-ring data up to 2018 CE (Figure 1). For the updated and new collections, we followed standard dendrochronological methods in the sampling and sample preparation (Supporting Information S1; Stokes & Smiley, 1968).

## 2.3. Reconstruction Model

We followed standard methods to develop our reconstruction model, using a principal component regression (Cook et al., 1999) to reconstruct the streamflow variables of our target gauge data (Supporting Information S1). Tree-ring reconstructions often underestimate both high and low extremes, leading to different biases in the tails of the distribution. A method to bias-correct streamflow reconstructions (with both high and low biases) of the Colorado River presents a way to improve estimates of past streamflow (Robeson et al., 2020). Therefore, we bias-corrected the reconstruction model with the highest variance explained (59%), the baseflow reconstruction (Supporting Information S1).

## 2.4. Species Contribution to Reconstructions

We examined each species contribution to the reconstruction model by calculating the absolute beta weights for each chronology that was used in the three streamflow metric reconstructions. For an individual chronology that had both the  $t$  and  $t+1$  chronologies retained as predictors in a given model, we summed the beta weights for that chronology. For every species comprising more than one chronology in the streamflow metric reconstructions, we calculated the percentage of all the summed beta weights for each separate chronology and averaged those percentages across all chronologies from the same species to get the average relative explained variance for that species.

## 2.5. Climate Analyses

To determine the possible influence of large-scale atmospheric-oceanic modes of variability in the streamflow metrics, we compared streamflow with climate indices that have been shown to influence precipitation and streamflow in the southeastern US. We focused on the bivariate ENSO index (BEST; 1948–2018 CE; Smith & Sardeshmukh, 2000), the Atlantic Multidecadal Variability (1856–2018 CE; Enfield et al., 2001), and the Bermuda High Index (BHI; 1948–2018 CE; Katz et al., 2003; Ortegren et al., 2011). We then performed correlations analyses between all climate indices and each streamflow metric reconstruction over their period of overlap. We also conducted spatial correlation analyses with gridded 850-hPa meridional wind (1948–2018 CE) from the NCEP/NCAR Reanalysis, which can indicate the location of the western flank of the North American

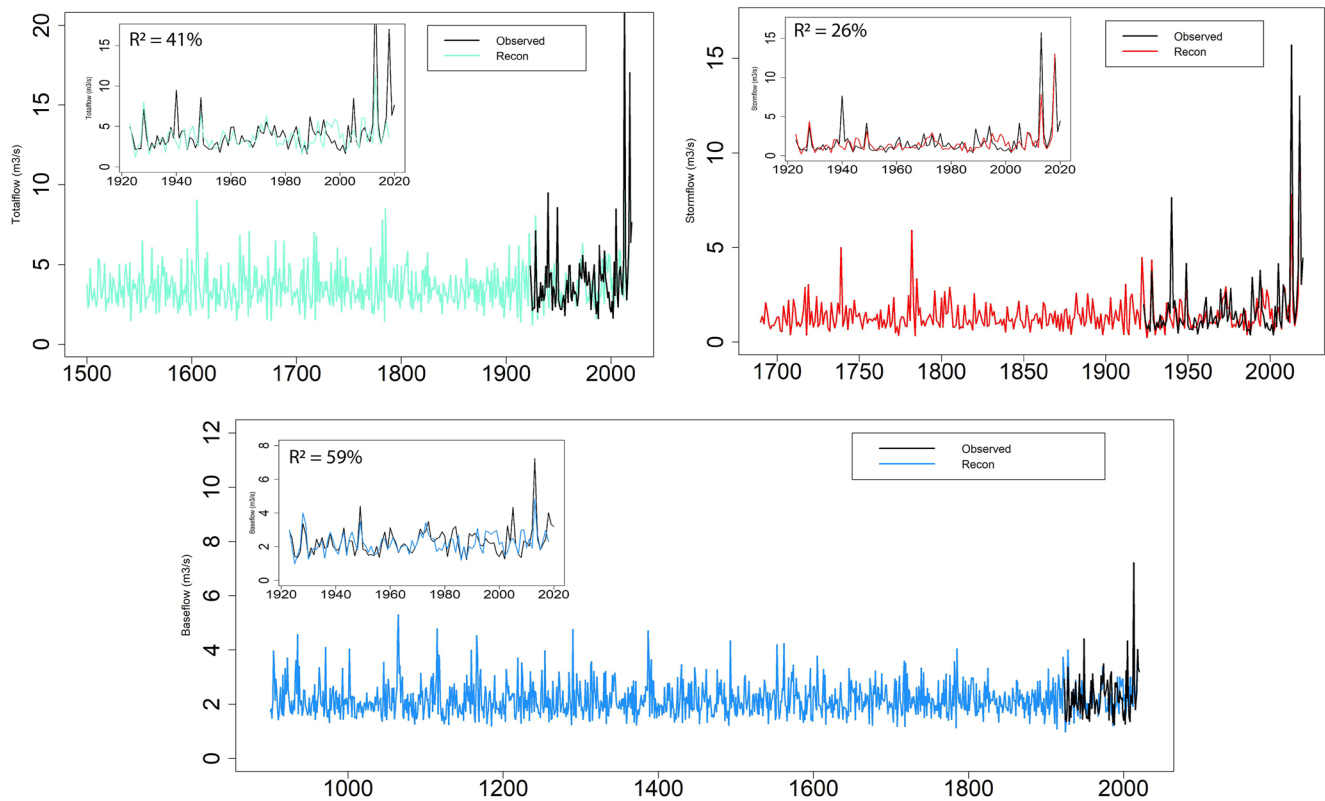


**Figure 2.** Varied tree-ring based Santee River reconstructions. Time series showing reconstruction of mean annual discharge ( $\text{m}^3/\text{s}$ ) for streamflow (mint green), stormflow (red), and baseflow (blue) compared to the observed discharge (black). Length of the reconstruction was determined by the earliest nested reconstruction model that could explain greater than 20% (see Supporting Information S1). Inset is a time series of reconstructed and observed for the instrumental record (1923–2018 CE).

subtropical high (NASH; Li et al., 2011; Li, Li, Ting, & Liu, 2012) on streamflow variability using KNMI climate explorer (Trouet and Van Oldenborgh, 2013). We gathered gridded sea surface temperatures (SSTs) for the North Atlantic from the Hadley Center (1850–2018 CE; Kennedy et al., 2011) for the period 1850 through 2018 and performed a spatial correlation with our streamflow reconstructions. We further compared our streamflow metric reconstructions with reconstructions of climate indices including: The North Atlantic Oscillation (summer; Folland et al., 2009), annual ENSO (Braganza et al., 2009), winter ENSO (W. Li, Li et al., 2013; J. Li, Xie et al., 2013), and tropical North Atlantic SSTs (April–March tropical year; Tierney et al., 2015).

### 3. Results

Radial growth from tree rings in the southeastern US responded stronger to baseflow than to stormflow and streamflow (Figure 2). The baseflow reconstruction explained 59% of the variance during the most replicated nest (see Supporting Information S1) compared to 26% and 41% for stormflow and streamflow, respectively (Tables S1–S3 in Supporting Information S1). Due to superior model statistics, the baseflow reconstruction extended to 900 CE before performance drops below 20%, while the stormflow and streamflow reconstructions were temporally shorter and statistically weaker, maintaining sufficient explanatory power back to 1690 and 1500 CE, respectively (Figure 2; Tables S1–S3 in Supporting Information S1).

The millennial-length baseflow record was mainly driven by the long-lived *Taxodium distichum* (bald cypress) (Tables S4 and S6 in Supporting Information S1; Tables S5 and S7). Different species appeared to capture different aspects of streamflow, with radial growth of *T. distichum* being the most important to the baseflow reconstruction and *Quercus montana* (chestnut oak) being the most important to the stormflow reconstruction (Table S4 in Supporting Information S1).

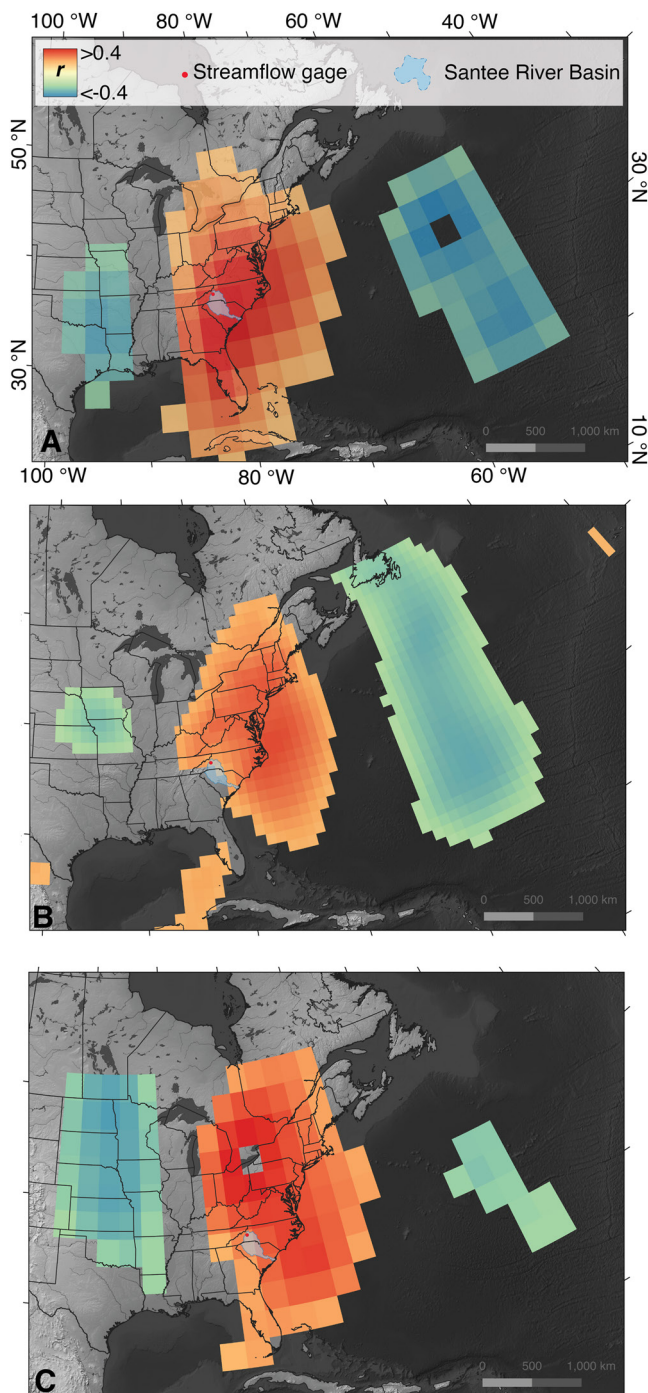


**Figure 3.** Atmospheric controls on Santee River baseflow. Spatial correlation between the instrumental (a) and bias-corrected reconstructed (b) baseflow and  $2.5^\circ$  gridded average May–August 850-hPa meridional wind from NCEP/NCAR Reanalysis (1948–2020 CE). Spatial correlation between the bias-corrected reconstructed baseflow and  $1^\circ$  gridded average May–August 850-hPa meridional wind from the 20th Century Reanalysis (1836–2015 CE; c).

While tree-ring chronologies best represented the baseflow reconstruction, even here the tree-ring estimates of baseflow had both negative and positive biases. The bias-correction procedure produced a reconstruction that decreases the lowest extremes and increases the higher extremes to better match the instrumental record (Figure S5 in Supporting Information S1). The bias-correction of the reconstruction allowed for the direct comparison of instrumentally recorded baseflow in more recent years allowing us to add the years 2019 and 2020 CE to the overall record, resulting in a time series of baseflow from 900 to 2020 CE (Figure S5 in Supporting Information S1). Baseflow over the reconstruction had a weak increasing trend (Sen's slope =  $0.007 \text{ m}^3/\text{s}/\text{century}$ ,  $p = 0.061$ ). However, two of the top 10 highest seasonal baseflow levels were in the instrumental record (1949 and 2013 CE), with 2013 CE having the largest baseflow ( $4.8 \text{ m}^3/\text{s}$ ) level over the last ca. 1,100 years. These high baseflow levels along with heavy rains created one of the worst flooding events in the upper reaches of the Linville and Catawba Rivers (tributaries of the Santee River).

When examining the potential larger-scale climate controls on the Santee River baseflow, we found that the only significant correlation with any of the climatic indices is with the BHI. Instrumental baseflow has a higher correlation ( $r = 0.45$ ;  $p < 0.01$ ) than the reconstructed baseflow ( $r = 0.23$ ;  $p < 0.05$ ) with average May–August BHI but both show a positive relationship. Further, when examining the May–August average 850-hPa meridional wind from the NCEP/NCAR reanalysis (1948–2020 CE), the  $2.5^\circ$  grids offshore the Mid-Atlantic coast are significantly positively correlated with Santee River baseflow (Figure 3), indicating that stronger meridional winds yield higher baseflow. The 850-hPa meridional winds could be used to indicate the location western flank of the NASH (Li et al., 2011; Li, Li, Ting, & Liu, 2012) and provided further evidence of the connections between the subtropical high pressure and seasonal averages of baseflow, likely due to the ability of the NASH to track moisture and storms (Bregy et al., 2020; Katz et al., 2003) into the watershed of the Santee River.

#### 4. Discussion

Paleoclimatic perspectives of streamflow using tree rings provide insight into multi-decadal and multi-centennial variability of streamflow that is not apparent in the instrumental record (Stockton & Jacoby, 1976; Wise, 2010; Woodhouse et al., 2006). However, examination on the efficacy of using tree rings to reconstruct theoretical baseflow and stormflow is limited, with only one example of the Potomac River suggesting that tree rings are more representative of baseflow (Torbensohn & Stagge, 2021). Here, we found supporting evidence that tree rings better represent baseflow for the Santee River and provide the longest baseflow reconstruction to date.

By employing the *climate footprint* method to screen sensitive chronologies that experience similar seasonal hydroclimate variability in the watershed (Harley et al., 2017; Maxwell et al., 2017), it allowed a larger pool of tree-ring chronologies to be used in the reconstruction. This approach allowed for the inclusion of multiple *T. distichum* records (Stahle & Cleaveland, 1992), which appeared to increase the performance of the baseflow reconstruction (Table S4 in Supporting Information S1). *T. distichum* grows in swamps in the southeastern US and are often inundated, and similar tree species growing in the floodplain around the world are an important source of evapotranspiration of local baseflow (Carmichael et al., 2018). Because of their low placement in the floodplain, *T. distichum* likely responds to flows

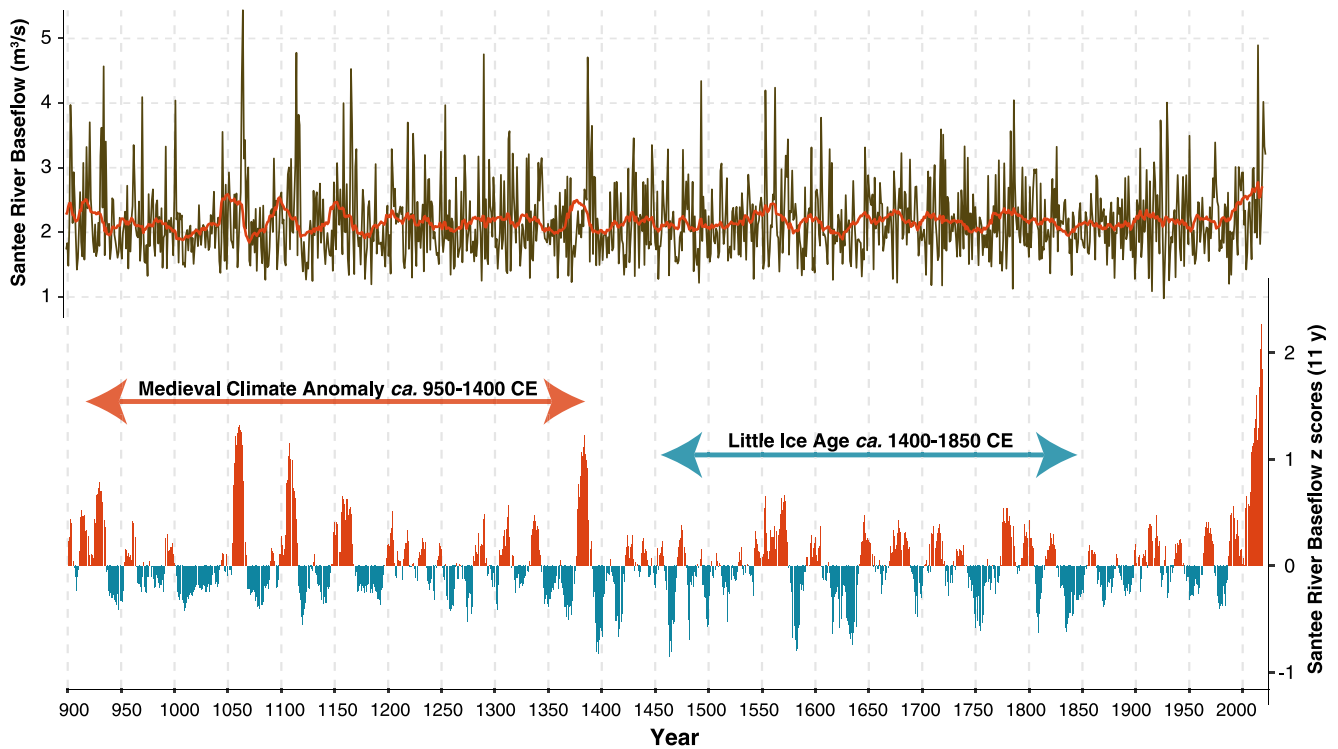


**Figure 4.** Long-term variability of Santee River baseflow. Time series of the bias-corrected baseflow reconstruction for the Santee River with a 20-year loess spline (top). Z scores of the bias-corrected baseflow, illustrating long term variability in baseflow through time (bottom).

of groundwater as compared to species growing higher in the floodplain and would be more likely to correlate with baseflow. Thus, targeted sampling could improve paleoclimatic estimates of baseflow, particularly throughout the range of *T. distichum* in the southeastern US. Conversely, we see species that grow in permeable or shallow soils (e.g., *Q. stellata* and *Q. montana*; Campbell, 1965) or have shallow roots (*Liriodendron tulipifera*; Francis, 1979) as more important to the stormflow model, albeit with lower  $R^2$  values compared to the baseflow reconstruction model (Table S4 in Supporting Information S1).

Overall, we see a pattern of higher baseflow maxima during the Medieval Climate Anomaly (ca. 950–1400 CE) and a period of elevated temperature for the study region; Mann et al., 2009), lower baseflow minima during the Little Ice Age (ca. 1400–1850 CE; a period of lower temperatures; Mann et al., 2009), and extremely high baseflow maxima since ca. 2000 CE (Figure 4). The highest baseflow value (2013 CE;  $4.8 \text{ m}^3/\text{s}$ ) occurs in the observed record (1923–2018 CE), and two other high ( $>4.0 \text{ m}^3/\text{s}$ ) baseflow years occur in 1949 and 2005 CE, producing an annual recurrence probability of 3.1%. High periods exceeding those years in the observed record within the 1,100-year reconstruction existed in nine other years, producing an annual recurrence probability 0.9%. Baseflow values above  $4.0 \text{ m}^3/\text{s}$  occurred more frequently in the observed record than at any other period in the reconstruction (Figure 4).

One of the dominant controls on summer precipitation variability in the southeastern US is the western flank of the NASH (Katz et al., 2003; W. Li et al., 2011; L. Li, Li, & Kushnir, 2012; W. Li, Li et al., 2013; J. Li, Xie et al., 2013). The semi-persistent anticyclone is generally located between Bermuda and the Azores (Davis et al., 1997). The location of the western flank as measured by the BHI is known to have a strong influence on drought occurrence throughout the southeastern US as well (Ortegren et al., 2014). Thus, it is unsurprising that we see a strong connection between reconstructed baseflow of the Santee River to the BHI and 850-hPa meridional winds along the east coast, which are representative of the location of the western flank of the NASH.

Subtropical highs in the northern hemisphere are intensifying and this is at least partially explained by the warming of the planet (Li, Li, Ting, & Liu, 2012). The intensification of the NASH results in a westward shift in the western flank, bringing more consistent rain into the region and increasing baseflow (Figure 4). We see a similar situation during the Medieval Climate Anomaly, where we see higher baseflow maxima, likely due to a more

westward shift in the mean position in the NASH during that time (Figure 4). Conversely, during the Little Ice Age, a weaker and more eastward shift in the NASH likely led to some of the lowest baseflow values in the reconstruction. With temperatures projected to continue to increase in the northern hemisphere, higher unprecedented baseflow maximums are likely to occur in the future for the Santee River. Higher baseflows could lead to more water in the Santee River, which when combined with heavy rainfall events, could lead to higher flooding levels. The severity-duration analysis demonstrates how wet the recent period has been compared to the entire reconstruction, with the wettest 2-year and 7-year periods and the third wettest 5-year period occurring since the 1970s (Figure S6 in Supporting Information S1).

## 5. Conclusions

We produced a 1,100-year reconstruction of baseflow for the Santee River using tree-ring chronologies selected based on a *climate footprint* approach. Our reconstruction model explained 59% of instrumental baseflow variance for the Linville River gauge. The reconstruction incorporated up to 64 chronologies from the surrounding region from eight species. Variability in seasonal baseflow levels was best represented by tree species lowest in the floodplain (e.g., *T. distichum*), while tree species with shallow root systems and shallow soils responded better to stormflow (e.g., *L. tulipifera* and *Q. stellata*). The bias-correction procedure adjusted both high and low biases in the extremes, showing that this procedure better represents extremes in baseflow reconstructions.

The western flank of the NASH is an important driver for precipitation in this region, and instrumental baseflow used in this study is linked to the BHI from May to August ( $r = 0.45$ ;  $p < 0.01$ ). Additionally, our reconstruction suggests that during the 1,100-year period, baseflow has significantly increased with time. Considering the increase in extreme precipitation events for the region, baseflow (thus, groundwater) will play a pivotal role in localized flooding during storm events in the future. Future exploration of streamflow reconstructions should consider (a) the relationship of baseflow and stormflow against the predictand proxy, (b) the opportunity provided by tree species occupying lowland areas, and (c) the role of large climate controls on basin-wide hydrologic characteristics.

## Data Availability Statement

The tree-ring chronologies from this paper—a list of which is included on Table S6 in Supporting Information S1; Tables S5 and S7 updated to the year 2018—are archived at the International Tree-Ring Data Bank (<https://www.ncei.noaa.gov/products/paleoclimatology/tree-ring>).

## Acknowledgments

We would like to thank April Kaiser, Torrin Kray-Mawhor, and B Tucker Rusty for assistance in the field and laboratory. We would also like to acknowledge funding from the U.S. National Science Foundation Paleo Perspectives on Climate Change, P2C2 Program (AGS-1805617, 1805959, 1805276, 2002524, and 2002482). We thank two anonymous reviewers for offering comments and suggestions that improved earlier drafts of this manuscript.

## References

- Ban, N., Schmidli, J., & Schär, C. (2015). Heavy precipitation in a changing climate: Does short-term summer precipitation increase faster? *Geophysical Research Letters*, 42(4), 1165–1172. <https://doi.org/10.1002/2014GL062588>
- Braganza, K., Gergis, J. L., Power, S. B., Risbey, J. S., & Fowler, A. M. (2009). A multiproxy index of the El Niño–Southern Oscillation, A.D. 1525–1982. *Journal of Geophysical Research*, 114(D5), D05106. <https://doi.org/10.1029/2008JD010896>
- Bregy, J. C., Maxwell, J. T., Robeson, S. M., Ortegren, J. T., Soulé, P. T., & Knapp, P. A. (2020). Spatiotemporal variability of tropical cyclone precipitation using a high-resolution, gridded ( $0.25^\circ \times 0.25^\circ$ ) dataset for the eastern United States, 1948–2015. *Journal of Climate*, 33(5), 1803–1819. <https://doi.org/10.1175/JCLI-D-18-0885.1>
- Campbell, R. A. (1965). Scarlet oak (*Quercus coccinea* Muenchh). In H. A. Fowells (Ed.), *Silvics of forest trees of the United States. Agriculture handbook 271* (pp. 611–614). U.S. Department of Agriculture. Comp.
- Carmichael, M. J., White, J. C., & Smith, W. K. (2018). Water source utilization in taxodium distichum (L.) Rich. (baldcypress) over the course of a growing season in a restored coastal freshwater wetland vulnerable to saltwater incursion. *Castanea*, 83(2), 272–287. <https://doi.org/10.2179/18-158>
- Cook, E. R., & Jacoby, G. C. (1977). Tree-ring-drought relationships in the Hudson Valley, New York. *Science*, 198(4315), 399–401. <https://doi.org/10.1126/science.198.4315.399>
- Cook, E. R., & Jacoby, G. C. (1983). Potomac river streamflow since 1730 as reconstructed by tree rings. *Journal of Applied Meteorology and Climatology*, 22(10), 1659–1672. [https://doi.org/10.1175/1520-0450\(1983\)022<1659:PRSSAR>2.0.CO;2](https://doi.org/10.1175/1520-0450(1983)022<1659:PRSSAR>2.0.CO;2)
- Cook, E. R., Meko, D. M., Stahle, D. W., & Cleaveland, M. K. (1999). Drought reconstructions for the continental United States. *Journal of Climate*, 12(4), 1145–1162. [https://doi.org/10.1175/1520-0442\(1999\)012<1145:DRFTCU>2.0.CO;2](https://doi.org/10.1175/1520-0442(1999)012<1145:DRFTCU>2.0.CO;2)
- Davis, R. E., Hayden, B. P., Gay, D. A., Phillips, W. L., & Jones, G. V. (1997). The north Atlantic subtropical anticyclone. *Journal of Climate*, 10(4), 728–744. [https://doi.org/10.1175/1520-0442\(1997\)010<0728:TNASA>2.0.CO;2](https://doi.org/10.1175/1520-0442(1997)010<0728:TNASA>2.0.CO;2)
- Enfield, D. B., Mestas-Núñez, A. M., & Trimble, P. J. (2001). The Atlantic multidecadal oscillation and its relation to rainfall and river flows in the continental U.S. *Geophysical Research Letters*, 28(10), 2077–2080. <https://doi.org/10.1029/2000GL012745>
- Folland, C. K., Knight, J., Linderholm, H. W., Fereday, D., Ineson, S., & Hurrell, J. W. (2009). The summer north Atlantic oscillation: Past, present, and future. *Journal of Climate*, 22(5), 1082–1103. <https://doi.org/10.1175/2008JCLI2459.1>



- Francis, J. K. (1979). *Yellow-poplar rooting habits*. Research Note SO-246. U.S. Department of Agriculture, Forest Service, Southern Forest Experiment Station. (p. 3).
- Gangrade, S., Kao, S.-C., & McManamay, R. A. (2020). Multi-model hydroclimate projections for the Alabama-Coosa-Tallapoosa River Basin in the southeastern United States. *Scientific Reports*, *10*(1), 2870. <https://doi.org/10.1038/s41598-020-59806-6>
- Hall, T. M., & Kossin, J. P. (2019). Hurricane stalling along the North American coast and implications for rainfall. *NPI Climate and Atmospheric Science*, *2*(1), 1–9. <https://doi.org/10.1038/s41612-019-0074-8>
- Harley, G. L., & Maxwell, J. T. (2018). Current declines of Pecos River (New Mexico, USA) streamflow in a 700-year context. *The Holocene*, *28*(5), 767–777. <https://doi.org/10.1177/0959683617744263>
- Harley, G. L., Maxwell, J. T., Larson, E., Grissino-Mayer, H. D., Henderson, J., & Huffman, J. (2017). Suwannee river flow variability 1550–2005 CE reconstructed from a multispecies tree-ring network. *Journal of Hydrology*, *544*, 438–451. <https://doi.org/10.1016/j.jhydrol.2016.11.020>
- Harris, I., Osborn, T. J., Jones, P., & Lister, D. (2020). Version 4 of the CRU TS monthly high-resolution gridded multivariate climate dataset. *Scientific Data*, *7*(1), 109. <https://doi.org/10.1038/s41597-020-0453-3>
- Kannenberg, S. A., Maxwell, J. T., Pederson, N., D'Orangeville, L., Ficklin, D. L., & Phillips, R. P. (2019). Drought legacies are dependent on water table depth, wood anatomy and drought timing across the eastern US. *Ecology Letters*, *22*(1), 119–127. <https://doi.org/10.1111/ele.13173>
- Katz, R. W., Parlange, M. B., & Tebaldi, C. (2003). Stochastic modeling of the effects of large-scale circulation on daily weather in the southeastern US. In L. O. Mearns (Ed.), *Issues in the impacts of climate variability and change on agriculture: Applications to the southeastern United States* (pp. 189–216). Springer Netherlands. [https://doi.org/10.1007/978-94-017-1984-1\\_9](https://doi.org/10.1007/978-94-017-1984-1_9)
- Kennedy, J. J., Rayner, N. A., Smith, R. O., Parker, D. E., & Saunby, M. (2011). Reassessing biases and other uncertainties in sea surface temperature observations measured in situ since 1850: 1. Measurement and sampling uncertainties. *Journal of Geophysical Research*, *116*(D14), D14103. <https://doi.org/10.1029/2010JD015218>
- Li, J., Xie, S.-P., Cook, E. R., Morales, M. S., Christie, D. A., Johnson, N. C., et al. (2013). El Niño modulations over the past seven centuries. *Nature Climate Change*, *3*(9), 822–826. <https://doi.org/10.1038/nclimate1936>
- Li, L., Li, W., & Kushnir, Y. (2012). Variation of the North Atlantic subtropical high western ridge and its implication to Southeastern US summer precipitation. *Climate Dynamics*, *39*(6), 1401–1412. <https://doi.org/10.1007/s00382-011-1214-y>
- Li, W., Li, L., Fu, R., Deng, Y., & Wang, H. (2011). Changes to the North Atlantic subtropical high and its role in the intensification of summer rainfall variability in the southeastern United States. *Journal of Climate*, *24*(5), 1499–1506. <https://doi.org/10.1175/2010JCLI3829.1>
- Li, W., Li, L., Fu, R., Deng, Y., & Wang, H. (2013). Reply to “Comments on ‘Changes to the north Atlantic subtropical high and its role in the intensification of summer rainfall variability in the southeastern United States’”. *Journal of Climate*, *26*(2), 683–688. <https://doi.org/10.1175/JCLI-D-11-00674.1>
- Li, W., Li, L., Ting, M., & Liu, Y. (2012). Intensification of Northern Hemisphere subtropical highs in a warming climate. *Nature Geoscience*, *5*(11), 830–834. <https://doi.org/10.1038/ngeo1590>
- Mann, M. E., Zhang, Z., Rutherford, S., Bradley, R. S., Hughes, M. K., Shindell, D., et al. (2009). Global signatures and dynamical origins of the Little Ice Age and Medieval Climate Anomaly. *Science*, *326*(5957), 1256–1260. <https://doi.org/10.1126/science.1177303>
- Maxwell, J. T., Bregy, J. C., Robeson, S. M., Knapp, P. A., Soulé, P. T., & Trouet, V. (2021). Recent increases in tropical cyclone precipitation extremes over the US east coast. *Proceedings of the National Academy of Sciences*, *118*(41), e2105636118. <https://doi.org/10.1073/pnas.2105636118>
- Maxwell, R. S., Harley, G. L., Maxwell, J. T., Rayback, S. A., Pederson, N., Cook, E. R., et al. (2017). An interbasin comparison of tree-ring reconstructed streamflow in the eastern United States. *Hydrological Processes*, *31*(13), 2381–2394. <https://doi.org/10.1002/hyp.11188>
- Maxwell, R. S., Hessler, A. E., Cook, E. R., & Pederson, N. (2011). A multispecies tree ring reconstruction of Potomac River streamflow (950–2001). *Water Resources Research*, *47*(5). <https://doi.org/10.1029/2010WR010019>
- Meehl, G. A., Arblaster, J. M., & Chung, C. T. Y. (2015). Disappearance of the southeast U.S. “warming hole” with the late 1990s transition of the Interdecadal Pacific Oscillation. *Geophysical Research Letters*, *42*(13), 5564–5570. <https://doi.org/10.1002/2015GL064586>
- Nagy, R. C., Lockaby, B. G., Helms, B., Kalin, L., & Stoeckel, D. (2011). Water resources and land use and cover in a humid region: The southeastern United States. *Journal of Environmental Quality*, *40*(3), 867–878. <https://doi.org/10.2134/jeq2010.0365>
- Ortega, J. T., Knapp, P. A., Maxwell, J. T., Tyminski, W. P., & Soulé, P. T. (2011). Ocean-atmosphere influences on low-frequency warm-season drought variability in the Gulf Coast and southeastern United States. *Journal of Applied Meteorology and Climatology*, *50*(6), 1177–1186. <https://doi.org/10.1175/2010JAMC2566.1>
- Ortega, J. T., Weatherall, A., & Maxwell, J. T. (2014). Subregionalization of low-frequency summer drought variability in the southeastern United States. *The Professional Geographer*, *66*(2), 323–332. <https://doi.org/10.1080/00330124.2013.787008>
- Robeson, S. M., Maxwell, J. T., & Ficklin, D. L. (2020). Bias correction of paleoclimatic reconstructions: A new look at 1, 200+ years of upper Colorado River flow. *Geophysical Research Letters*, *47*(1), e2019GL086689. <https://doi.org/10.1029/2019GL086689>
- Seager, R., Tzanova, A., & Nakamura, J. (2009). Drought in the southeastern United States: Causes, variability over the last millennium, and the potential for future hydroclimate change. *Journal of Climate*, *22*(19), 5021–5045. <https://doi.org/10.1175/2009JCLI2683.1>
- Slack, J. R., & Landwehr, J. M. (1992). *Hydro-climatic data network (HCDN); a U.S. Geological survey streamflow data set for the United States for the study of climate variations, 1874-1988 (USGS numbered series no. 92-129)*. Hydro-climatic data network (HCDN); a U.S. Geological survey streamflow data set for the United States for the study of climate variations (Vol. 92–129, pp. 1874–1988). U.S. Geological Survey; Copies of this report can be purchased from USGS Books and Open-File Reports Section. <https://doi.org/10.3133/ofr92129>
- Sloto, R., & Crouse, M. (1996). HYSEP-A computer program for streamflow hydrograph separation and analysis. *United States Geological Survey Water-Resources Investigations Report*, *96*, 4040.
- Smith, C. A., & Sardeshmukh, P. D. (2000). The effect of ENSO on the intraseasonal variance of surface temperatures in winter. *International Journal of Climatology*, *20*(13), 1543–1557. [https://doi.org/10.1002/1097-0088\(20001115\)20:13<1543::AID-JOC579>3.0.CO;2-A](https://doi.org/10.1002/1097-0088(20001115)20:13<1543::AID-JOC579>3.0.CO;2-A)
- Stahle, D. W., & Cleaveland, M. K. (1992). Reconstruction and analysis of spring rainfall over the past 1000 years. *Bulletin of the American Meteorological Society*, *73*(12), 1947–1961. [https://doi.org/10.1175/1520-0477\(1992\)073<1947:raoosr>2.0.co;2](https://doi.org/10.1175/1520-0477(1992)073<1947:raoosr>2.0.co;2)
- Stockton, C. W., & Jacoby, G. C. (1976). Long-term surface-water supply and streamflow trends in the Upper Colorado River basin based on tree-ring analyses. *Lake Powell Research Project Bulletin*, *18*, 70.
- Stokes, M. A., & Smiley, T. L. (1968). *An introduction to tree-ring dating*. University of Arizona Press.
- Strange, B. M., Maxwell, J. T., Robeson, S. M., Harley, G. L., Therrell, M. D., & Ficklin, D. L. (2019). Comparing three approaches to reconstructing streamflow using tree rings in the Wabash River basin in the Midwestern, US. *Journal of Hydrology*, *573*, 829–840. <https://doi.org/10.1016/j.jhydrol.2019.03.057>
- Tierney, J. E., Abram, N. J., Anchukaitis, K. J., Evans, M. N., Giry, C., Kilbourne, K. H., et al. (2015). Tropical sea surface temperatures for the past four centuries reconstructed from coral archives. *Paleoceanography*, *30*(3), 226–252. <https://doi.org/10.1002/2014PA002717>

- Torbenson, M. C. A., & Stagge, J. H. (2021). Informing seasonal proxy-based flow reconstructions using baseflow separation: An example from the Potomac River, United States. *Water Resources Research*, *57*(2), e2020WR027706. <https://doi.org/10.1029/2020WR027706>
- Trenberth, K. E., Dai, A., Rasmussen, R. M., & Parsons, D. B. (2003). The changing character of precipitation. *Bulletin of the American Meteorological Society*, *84*(9), 1205–1218. <https://doi.org/10.1175/BAMS-84-9-1205>
- Trepanier, J. C., & Tucker, C. S. (2018). Event-based climatology of tropical cyclone rainfall in Houston, Texas and Miami, Florida. *Atmosphere*, *9*(5), 170. <https://doi.org/10.3390/atmos9050170>
- Trouet, V., & Oldenborgh, G. J. V. (2013). KNMI climate explorer: A web-based research tool for high-resolution paleoclimatology. *Tree-Ring Research*, *69*(1), 3–13. <https://doi.org/10.3959/1536-1098-69.1.3>
- USGCRP. (2018). *Fourth national climate assessment* (pp. 1–470). U.S. Global Change Research Program. Retrieved from <https://nca2018.globalchange.gov>
- Vines, M., Tootle, G., Terry, L., Elliott, E., Corbin, J., Harley, G. L., et al. (2021). A paleo perspective of Alabama and Florida (USA) interstate streamflow. *Water*, *13*(5), 657. <https://doi.org/10.3390/w13050657>
- Wise, E. K. (2010). Tree ring record of streamflow and drought in the upper Snake River. *Water Resources Research*, *46*(11). <https://doi.org/10.1029/2010WR009282>
- Woodhouse, C. A., Gray, S. T., & Meko, D. M. (2006). Updated streamflow reconstructions for the Upper Colorado River Basin. *Water Resources Research*, *42*(5). <https://doi.org/10.1029/2005WR004455>

## References From the Supporting Information

- Bussberg, N. W., Maxwell, J. T., Robeson, S. M., & Huang, C. (2020). The effect of end-point adjustments on smoothing splines used for tree-ring standardization. *Dendrochronologia*, *60*, 125665. <https://doi.org/10.1016/j.dendro.2020.125665>
- Cook, E. R. (1985). *A time series analysis approach to tree ring standardization*. PhD thesis. University of Arizona.
- Cook, E. R., & Peters, K. (1981). The smoothing spline: A new approach to standardizing forest interior tree-ring width series for dendroclimatic studies. Retrieved from <https://repository.arizona.edu/handle/10150/261038>
- Fritts, H. C. (1976). *Tree rings and climate*. Academic Press.
- González, J., & Valdés, J. B. (2003). Bivariate drought recurrence analysis using tree ring reconstructions. *Journal of Hydrologic Engineering*, *8*(5), 247–258. [https://doi.org/10.1061/\(ASCE\)1084-0699](https://doi.org/10.1061/(ASCE)1084-0699)
- Gudmundsson, L., Bremnes, J. B., Haugen, J. E., & Engen-Skaugen, T. (2012). Technical note: Downscaling RCM precipitation to the station scale using statistical transformations – a comparison of methods. *Hydrology and Earth System Sciences*, *16*(9), 3383–3390. <https://doi.org/10.5194/hess-16-3383-2012>
- Holmes, R. (1983). Computer-assisted quality control in tree-ring dating and measurement. *Tree-Ring Bulletin*, *43*, 69–78.
- Meko, D. (1997). Dendroclimatic reconstruction with time varying predictor subsets of tree indices. *Journal of Climate*, *10*(4), 687–696. [https://doi.org/10.1175/1520-0442\(1997\)010<0687:DRWTVP>2.0.CO;2](https://doi.org/10.1175/1520-0442(1997)010<0687:DRWTVP>2.0.CO;2)
- R Core Team. (2021). *R: A language and environment for statistical computing*. R Foundation for Statistical Computing. Retrieved from <https://www.R-project.org/>